Journal of Power Sources 244 (2013) 136–142

Contents lists available at SciVerse ScienceDirect

Journal of Power Sources

journal homepage: www.elsevier.com/locate/jpowsour

Interface phenomena between Li anode and lithium phosphate electrolyte for Li-ion battery

Santosh K.C. [a], Ka Xiong [a], Roberto C. Longo [a], Kyeongjae Cho [a,b,*]

[a] Department of Materials Science & Engineering, The University of Texas at Dallas, Richardson, TX 75080, USA
[b] WCU Multiscale Mechanical Design Division, School of Mechanical and Aerospace Engineering, Seoul National University, Seoul 151-742, Republic of Korea

HIGHLIGHTS

- Li-ion defect formation energy in bulk solid electrolyte (Li_3PO_4).
- Defect formation energy in Li/Li_3PO_4 interface is estimated.
- Detailed analysis of electronic structures of Li/Li_3PO_4 interface.
- Energy barrier of Li ion migration across the interface is estimated.

ARTICLE INFO

Article history:
Received 24 September 2012
Received in revised form
21 February 2013
Accepted 25 February 2013
Available online 2 April 2013

Keywords:
Interface
Lithium phosphate
Nudged elastic band method
Ionic conductivity
Density functional theory

ABSTRACT

First-principles calculations are performed to investigate interface properties, Li defects formation and migration mechanism across the interface between negative metal electrode and solid electrolyte (Li/γ-Li_3PO_4). We have analyzed the band alignment between Li and Li_3PO_4, interfacial charge distribution and electronic properties to elucidate the properties of the model interface. Our results show that the high Li-ion (Li^+) defect formation energy is determined by the Li metal Fermi level leading to low ionic conductivity of Li metal/electrolyte interface. The electronic structure study of this Li metal/Li_3PO_4 interface provides information on the Li defect formation and migration, which will help us to improve the ionic conductivity for future Li-ion battery.

1. Introduction

A lot of research activities have been focused on improving energy and power densities, and cycle life of Li-ion battery to meet the demand for various technological future devices [1,2]. Many works have been dedicated to understand the conduction phenomena of all components of the Li-ion cell. There is also a need of more focused research on, in particular, the interface phenomena between the electrodes and electrolyte. Among the current electrolytes, solid electrolytes have great advantages over the liquid and polymer electrolytes for microelectronics applications [3–6]. Recently, lithium phosphorous oxynitride (LiPON), developed by Oak Ridge National Laboratory (ORNL), has been intensively used, as an electrolyte in thin-film batteries [7–11]. Solid electrolyte Li_3PO_4 is one of the natural and synthetic crystalline materials of the LiPON family. Those electrolytes can be used in thin films because of its chemical and physical stability. However, the low ionic conductivity is the main hindrance of solid electrolytes for its commercial applications [12,13].

The Li_3PO_4 has three crystalline forms, labeled as α, β, and γ in the literature [13]. The crystal structure of α-Li_3PO_4 has not been fully determined yet, while the crystal structures of β- and γ-Li_3PO_4 are well known and have been observed experimentally. However, the activated transport measurement has been done mainly on γ-Li_3PO_4 [14,15], because the stable β form irreversibly transforms into γ form at high temperature (400–600 °C) [16–18]. The γ-Li_3PO_4 has an orthorhombic *Pnma* structure (#62), similar to the well-studied cathode materials – $LiFePO_4$ and $FePO_4$ [19]. There has been some previous theoretical research on bulk β- and γ-Li_3PO_4 as solid electrolyte [20] but there are no reports in the literature on the Li^+ diffusion phenomena across the electrode and electrolyte interface.

* Corresponding author. Department of Materials Science & Engineering, The University of Texas at Dallas, Richardson, TX 75080, USA.
E-mail address: kjcho@utdallas.edu (K. Cho).

0378-7753/$ – see front matter © 2013 Elsevier B.V. All rights reserved.
http://dx.doi.org/10.1016/j.jpowsour.2013.02.093

The structure of the interface determines to a large extent the performance of the battery, controlling the resistivity and mechanical stability of the interface during the charge and discharge cycles.

Li metal has the highest specific capacity, 3.86 A h g^{-1}, and volumetric capacity, 2.06 A h cm^{-3} [2], of all possible negative electrodes, making Li as an ideal reference negative electrode. However, the formation of dendrites, its high reactivity, and low reversibility have hindered its applicability in conventional batteries with liquid electrolytes [21]. Including the solid electrolyte in an all-solid-state device, Li metal can be used as negative electrode with a reduced dendrite formation during the cycle of charge and discharge, enhancing the safety. Indeed, all-solid-state lithium secondary batteries have many advantages over the currently used liquid electrolyte–lithium secondary batteries in terms of thermal stability, safety and mechanical stability under external shock and vibrations [22–27].

An ideal solid electrolyte would require a relatively high ionic conductivity with unity of transport number (ratio of ionic conductivity and sum of ionic and electronic conductivities), and it also needs to be stable in contact with lithium metal over a wide range of operating voltage (0–5 V). The ionic conductivity in crystalline Li_3PO_4 is approximately 10^{-6} S cm^{-1} [28]. However, a proper concentration of solid solutions could improve the ionic conductivity; the study of Li_4GeO_4–Li_3PO_4 system shows that the ionic conductivity increases up to 10^{-4}–10^{-5} S cm^{-1} [29]. The solid solution Li_4SiO_4–Li_3PO_4 [30] shows that mixing Li_4SiO_4 into Li_3PO_4 introduces a significant amount of Li interstitial defects, reducing the activation barrier for Li diffusion to adjacent neighboring sites, thus enhancing the ionic conductivity [14]. The interface phenomena will have significant impact on the Li ion conduction mechanisms of the Li ion battery because they provide sources or sinks for Li defects [20]. The interfacial quality between solid electrode and solid electrolyte is one of the most crucial aspects while fabricating all-solid-state lithium ion battery [31]. Several experimental studies have also been trying to add amorphous materials into the electrode to increase the interface area between the active materials and the electrolyte; it is found to improve the interface resistivity as well as the mechanical stability [32,33]. All-solid-state $Li/Li_3PO_4/LiCoO_2$ battery has been fabricated using pulsed laser deposition (PLD) grown Li_3PO_4 thin film and it shows excellent intercalation properties and electrochemical stability in the operating voltage range from 0 to 4.7 V vs Li/Li^+ [34].

Computational modeling of an electrode–electrolyte interface is both an interesting and challenging task to understand the detailed performance during electrochemical cycles. In addition to the bulk properties of electrodes or electrolytes, the quality of the interface between them plays a crucial role in enhancing electrochemical stability, performance, and overall battery safety [31,35]. However, the atomic level mechanisms of electrode–electrolyte interface, including Li ion transfer (Li^+) across the interface are lacking in the literature. The kinetics of Li^+ transfer provides an idea on the activation energy for Li ion transfer in anode–electrolyte interface or electrolyte–cathode interface. The activation energy is associated with the interfacial chemistry at the particular interface. One of the main challenges for Li-ion batteries is to gain a detailed understanding of the electrode–electrolyte interface to control and improve the Li ion diffusion mechanism.

In this work, we have considered Li metal as the negative electrode and Li_3PO_4 as a solid electrolyte with LiPON-type structure to model an all-solid state battery. We have studied the formation of Li defects across the Li/γ-Li_3PO_4 interface, the interface phenomena and interface charge analysis, and the interfacial barrier for Li migration. These results will help us to understand the mechanisms of Li defect formation, Li-ion migration and other interfacial properties of Li/Li_3PO_4 interface.

2. Methodology

Our first-principles calculations were performed within the framework of the density functional theory (DFT) [36–39], with plane wave basis sets and projector augmented wave (PAW) [40–42] pseudo-potentials, as implemented in the Vienna *Ab-initio* Simulation Package (VASP) [43]. The electronic wave functions were represented by plane wave basis with a cutoff energy of 450 eV. The exchange and correlation interactions were incorporated as a functional of generalized gradient approximation (GGA) [43–45]. In the defect calculations, the atoms were allowed to relax while the cell size and angles were kept fixed. The energy and forces were converged up to 10^{-4} eV and 0.01 eV $Å^{-1}$, respectively. A Monkhorst-Pack 2 × 2 × 2 k-point mesh was used for the self-consistent calculations whereas a 4 × 4 × 4 k-point mesh was used for the density of states (DOS) calculations to achieve higher accuracy for the interface model. In order to investigate the Li diffusion pathways and migration energy in Li/γ-Li_3PO_4, interface, we used nudged elastic band (NEB) method [46] implemented in VASP. Five intermediate images were generated between the initial and final positions and each image was allowed to relax until the maximum residual force was less than 0.01 eV $Å^{-1}$.

The calculations of defects and migration energy in the present work are based on the supercell approach [47], where an isolated defect is placed in a periodically repeated large cell. For the interface modeling, seven atomic layers of Li (001) and five unit layers of γ-Li_3PO_4 (010) are used. The choice of this direction is in accordance with the Li ion migration channel and the lowest activation energy barrier for the Li ion migration, as previously reported in the literature [14,15,29]. To form the interface supercell, we chose γ-Li_3PO_4 (010) with surface area of 51.67 $Å^2$ (4.926 Å × 10.490 Å) and Li (001) with surface area of and 49.26 $Å^2$ (4.963 Å × 09.926 Å). The supercell has 172 atoms, containing 82 Li, 72 oxygen and 18 phosphorous atoms (see Fig.1). The lattice mismatch is less than 5%, which introduces the lattice incoherency strain; it also influences to the stability of the interface. For the bulk study of γ-Li_3PO_4, a 1 × 2 × 2 (10.490 Å × 12.240 Å × 9.853 Å) supercell with 128 (Li = 48, O = 64 and P = 16) atoms were used.

We have removed a Li ion from the metal anode side and placed it as an interstitial atom at different sites in the electrolyte side, obtaining the Li defect formation energy and Li migration energy across the interface. The charge neutrality of the interface model is maintained since the overall charge of the interface is unchanged in this procedure.

3. Results and discussion

3.1. Defect formation energy

The defect migration mechanism of bulk γ-Li_3PO_4 has been studied by Holzwarth et al. They showed that the Li interstitial mechanism (E_m ~ 0.2 eV for interstitialcy type) is favored over the vacancy migration (E_m ~ 0.7 eV) in γ-Li_3PO_4 [14,15]. Once the favorable defect migration mechanism in the bulk solid electrolyte γ-Li_3PO_4 is understood, we want to know how easy is for the Li-ion to migrate from Li metal to the electrolyte in our interface model, as shown in Fig. 2(b).

The interface model is optimized in order to find the ground-state configuration. During the relaxation process, the atomic positions closer to the interface are perceptibly displaced. The atoms of the metal anode side are slightly shifted toward the interface to minimize the energetic mismatch whereas the atoms of the electrolyte undergo a relatively small displacement: The Li atoms at the interface move ~0.48 Å toward the interface region from the electrode side. Li atoms of the bulk-like region of the electrolyte do not change appreciably their positions (~0.06 Å) (Fig. 1).

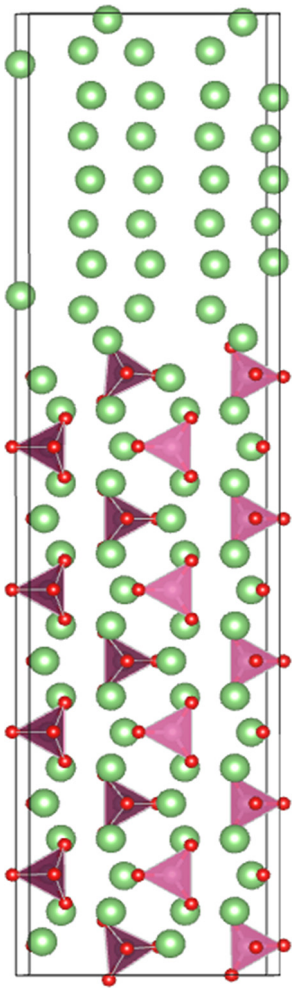

Fig. 1. The atomic structure of Li/γ-Li_3PO_4 interface. Li atoms are indicated by green spheres whereas PO_4 groups are indicated by red tetrahedra with red spheres (oxygen) at each corner (For interpretation of the references to color in this figure legend, the reader is referred to the web version of this article.).

In order to investigate how easy it would be for the Li-ion to migrate from the Li metal anode site to the interstitial sites of the electrolyte, we have created a Li vacancy (labeled with a red circle in Fig. 2(b)) in the Li electrode side and a Li interstitial defect at different sites of the electrolyte (green circles of Fig. 2(b)). The Li vacancy–interstitial defect formation energy in the Li (001)/Li_3PO_4 (010) interface is calculated using the following expression

$$E^{f}_{pair}\ (eV) = E_{defect(tot)} - E_{perfect(tot)} \quad (1)$$

where E^{f}_{pair} is the vacancy–interstitial pair defect formation energy, $E_{defect\ (tot)}$ is the total energy of the cell with the defect and $E_{perfect\ (tot)}$ is the total energy of the interface without defects.

The calculated Li vacancy–interstitial pair defect formation energies are summarized in Table 1. In our calculation, the position of Li vacancy in the electrode is fixed and the position of Li interstitial defect in the electrolyte varies as shown in Fig. 2(b). Our results show that the pair defect formation energy ranges from 0.82 eV to 1.93 eV. The first interstitial defect site is too close to the interface, being the formation energy negative due to the strong relaxation at the interface upon the creation of the defect. The obtained relaxed structure shows that after the relaxation, it goes back to the interface position to release the stress induced by the lattice mismatch. The results for the other interstitial defect sites show that the defect formation energy slightly increases as the defect moves away from the interface. However, the defect formation energy at site (4) is 1.58 eV, slightly lower than site (3). This site is approximately at the middle of the unit cell of the Li_3PO_4 electrolyte. Thus, it is a local minimum, and shows less interfacial effects. It attains the maximum value of 1.93 eV at the center of the electrolyte cell and then slightly decreases due to periodic boundary conditions (PBC).

Our results on defect formation energies show that the energy cost associated with the formation of defects across the hetero-junction of Li and Li_3PO_4 is relatively large for Li-ion battery purposes. To address this issue, we have also investigated the charged defect formation energy in the bulk electrolyte with a goal of understanding the formation energy profile with respect to the position of the Fermi level. The charged state defect formation energy is computed for bulk Li_3PO_4 using the following expression [19,48–50]:

$$E^{form}_{q} = E_{defect,q(tot)} - E_{perfect(tot)} - \sum_{i}\Delta n_i\mu_i + q(E_F + E_v + \Delta V) + E_{corr} \quad (2)$$

where E^{form}_{q} is the formation energy of a defect with charge q, Δn_i is the difference in the atom numbers ($\Delta n_i < 0$ if removed and $\Delta n_i > 0$ if added), μ_i is the chemical potential of species added or removed, E_F is Fermi energy, E_v is energy of the top of the valance band, ΔV is the difference in the local potential between the charged supercell and the neutral supercell in a position far from the defect site and E_{corr} is the dipole and quadrupole correction energies with proper scaling by the dielectric constant (ε). The chemical potential of Li is taken as that of the bulk value, −1.87 eV per atom as obtained in our calculations.

Fig. 3 shows the Li^+ defect formation energy plotted against the Fermi level across the band gap of bulk Li_3PO_4. It can be noted that the Li^+ interstitial formation energy dominates over the vacancy formation energy for a wide range of the Fermi energy in the band gap of Li_3PO_4. Thus, the Li^+ interstitial is likely to bring the most significant contribution to the ionic conductivity of this solid electrolyte. The formation energy of Li^+ is thus a function of the Fermi level. By tuning the Fermi level, we can control the defect formation energy: if E_f is lowered to 3 eV, Li^+ interstitial defects would form very easily. Moreover, for any value less than 3 eV, it results in the spontaneous formation of the Li^+ interstitial defect in the electrolyte. In our results, with the Fermi level at 4 eV, the Li ion interstitial formation energy is 1 eV. The activation energy barrier of our interface model could be reduced if the defect formation energy is lower than that of bulk electrolyte. When the interface is formed between Li metal and Li_3PO_4 electrolyte, they align to a common Fermi level. Thus, alloying Li metal can influence the overall Fermi level of the Li/L_3PO_4 interface and, as a result of it, the Li ion defect formation mechanism at the interface.

The use of Li alloy as the electrode would be a good direction for the research. However, there are other aspects that should be taken into account, like the volume change during charge and discharge which would result in cracking and crumbling of the electrode materials. This would cause capacity loss [51,52]. Therefore, careful alloying is suggested to avoid the rapid fade in the capacity upon cycling due to morphology deterioration during Li insertion and extraction [53]. Si and other metals like Sn, Sb, and Al could form promising alloys with metal Li in terms of high Li storage capacity [54]. A composite electrolyte of as $SiO_{1.1}$–$Li_{2.6}Co_{0.4}N$ has also shown an improved safety over the metallic Li batteries [55].

3.2. Interface charge analysis

In this section, we evaluate some interfacial phenomena like charge distribution, electronic properties and band alignment of

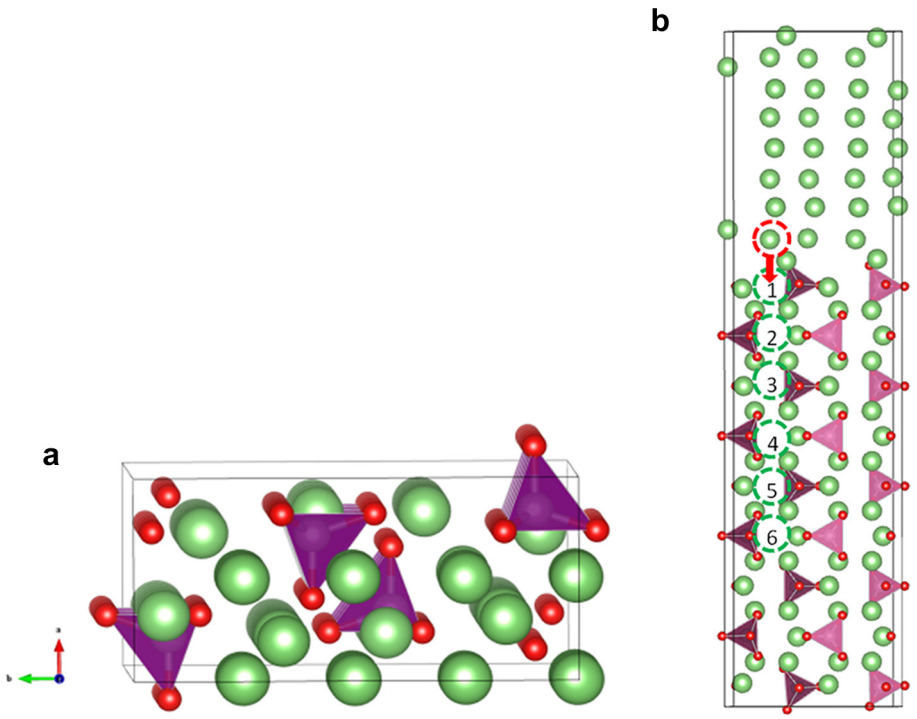

Fig. 2. Li (001)/Li_3PO_4 (010) interface (a) top view and (b) side view. The red circle represents the site of Li vacancy and green circles represent the Li interstitial sites, labeled from 1 to 6, respectively. Li-atoms are indicated by green spheres whereas the PO_4 groups are indicated by red tetrahedra with red spheres (oxygen) at each corner (For interpretation of the references to color in this figure legend, the reader is referred to the web version of this article.).

our interface model. Fig. 4(a) shows the interfacial charge distribution and electrostatic potential variation across the interface along *z*-direction from Li_3PO_4 electrolyte to Li metal side. Fig. 4(b) shows the charge density difference obtained for our interface model by subtracting the charge density of bulk Li and bulk Li_3PO_4 from that of Li/Li_3PO_4 interface, as given by equation (3):

$$\Delta\rho = \rho(\text{complex}) - \rho(\text{bulk } Li_3PO_4) - \rho(\text{bulk Li}) \quad (3)$$

The picture shows that there are some interfacial charge accumulation and depletion on the interface between Li and Li_3PO_4. The distance from 0 to 25 Å corresponds to Li_3PO_4 electrolyte and from 25 to 42 Å to the Li metal anode. The interface effect on the charge density profile can be noted in the region from 21 to 27 Å. The interface (25 Å) shows charge accumulation and, at 26.5 Å, there is charge depletion. This implies that the effect of the interface is reduced to a region of 4 Å inside the electrolyte. If this region is too deep, then, larger electrolyte thickness is needed or there even may be a chance for the electrons to flow from the electrode to the electrolyte (leakage) and short circuit of the device. Thus, this will directly affect the electronic (ionic) conductivity across the interface.

Based on the Bader charge analysis [56–58], we have investigated the charge states of the atoms in our interface model. Our calculations show that the bulk Li atoms contribute with 0.21 e (bulk electrode side) and 0.14 e charge (bulk electrolyte side), respectively, while at the interface, the Li atoms have 0.17 e, 0.42 e and 2.5 e depending on the nature of neighboring atomic environment like Li, PO_4 group or interstitial site of electrolyte. Thus, the electronic charges pile up on the Li atoms of electrode adjacent to Li_3PO_4 at the interface. The closest Li atom to the electrolyte PO_4 group shows the highest charge accumulation, while the Li atom closest to the interstitial site of the electrolyte at the interface shows the lowest charge state. The P atoms have 1.42 e in the bulk region and1.47 e at the interface. The O atoms show similar charge state at the interface and at the bulk-like region (7.5 e) due to its

Table 1
Li vacancy–interstitial defect formation energies in our model Li (001)/Li_3PO_4 (010) interface.

Label	Position of Li vacancy	Position of Li interstitial	E^{form} (eV)
(1)	[0.500, 0.253, 0.702]	[0.500, 0.250, 0.618]	−0.43
(2)		[0.500, 0.250, 0.545]	0.82
(3)		[0.500, 0.250, 0.472]	1.89
(4)		[0.500, 0.250, 0.400]	1.58
(5)		[0.500, 0.250, 0.327]	1.93
(6)		[0.500, 0.250, 0.254]	1.89

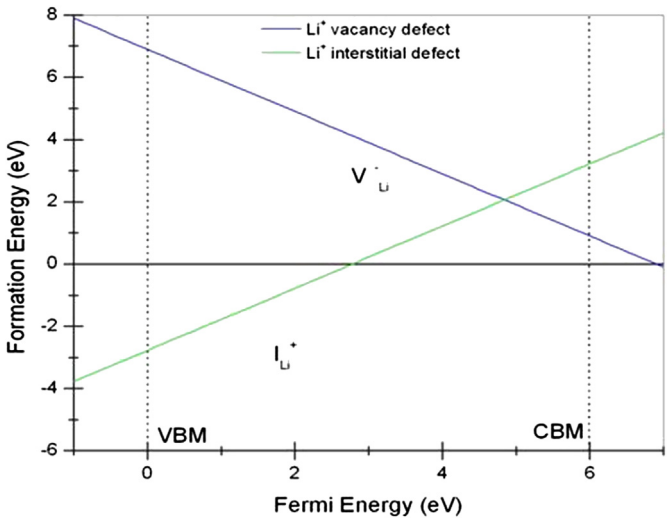

Fig. 3. Defect formation energies as a function of the Fermi energy of Li^+ interstitial and Li^+ vacancy defects in bulk Li_3PO_4.

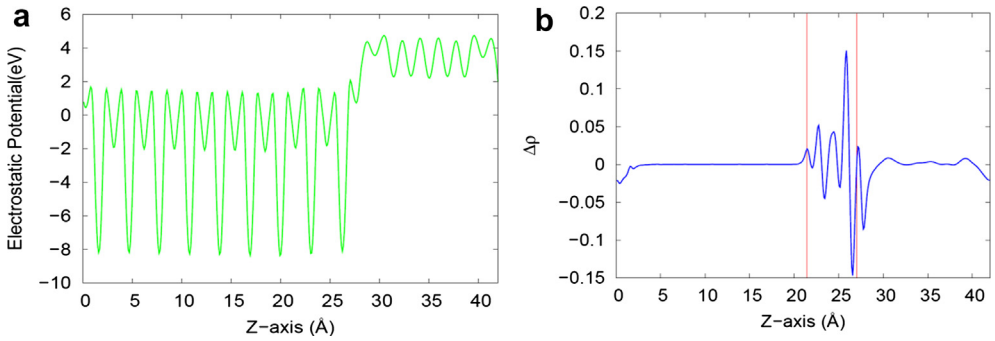

Fig. 4. (a) Variation of electrostatic potential and (b) charge difference along the z-direction (see text for details). Li metal and Li_3PO_4 interfaced at $Z = 25$ Å.

high electronegativity. Though this analysis does not provide an accurate description of the charge transfer process, it can provide an insight on the charge accumulation in Li_3PO_4 at the interface. Our results do not show changes in the charge states of atoms in electrolyte beyond the 4 Å away from the interface.

Fig. 5(b) shows the local density of states (DOS) projected at various atoms and at different layers away from the interface. The DOS labeled Li(1), Li(2) and Li(3) are those of metal Li, with Li(1) closer to the interface; the DOS of the different electrolyte layers are shown from layer (1) to layer (7), with layer (1) closer to the interface. The Fermi level is aligned to the zero of energy. Thus, we can note that the DOS projected at the interface has states in the Fermi level and thus, does not have a clear band gap, resulting in a metallic character. Fig. 5(b) also shows that there are no electronic states at the Fermi level beyond the second layer. Moreover, the metallic nature of Li anode is clearly shown in the number of electronic states present at the Fermi level. Our results show that the interface has metallic character due to the states induced by Li metal in the bulk band gap of Li_3PO_4. The states in the band gap reduce significantly as we move from the interface to the second layer. These interface states do not propagate very deep into the electrolyte, since they are barely noticeable on the scale of the plot at the second layer, as shown in Fig. 5(b). Thus, the use of Li_3PO_4 as a solid electrolyte provides sufficient electronic insulation to avoid leakage of electrical current between the electrodes through the electrolyte. Of course, the thickness of the electrolyte should be taken into account when micro scale batteries are designed since the self-discharge rate increases substantially for a thickness of few

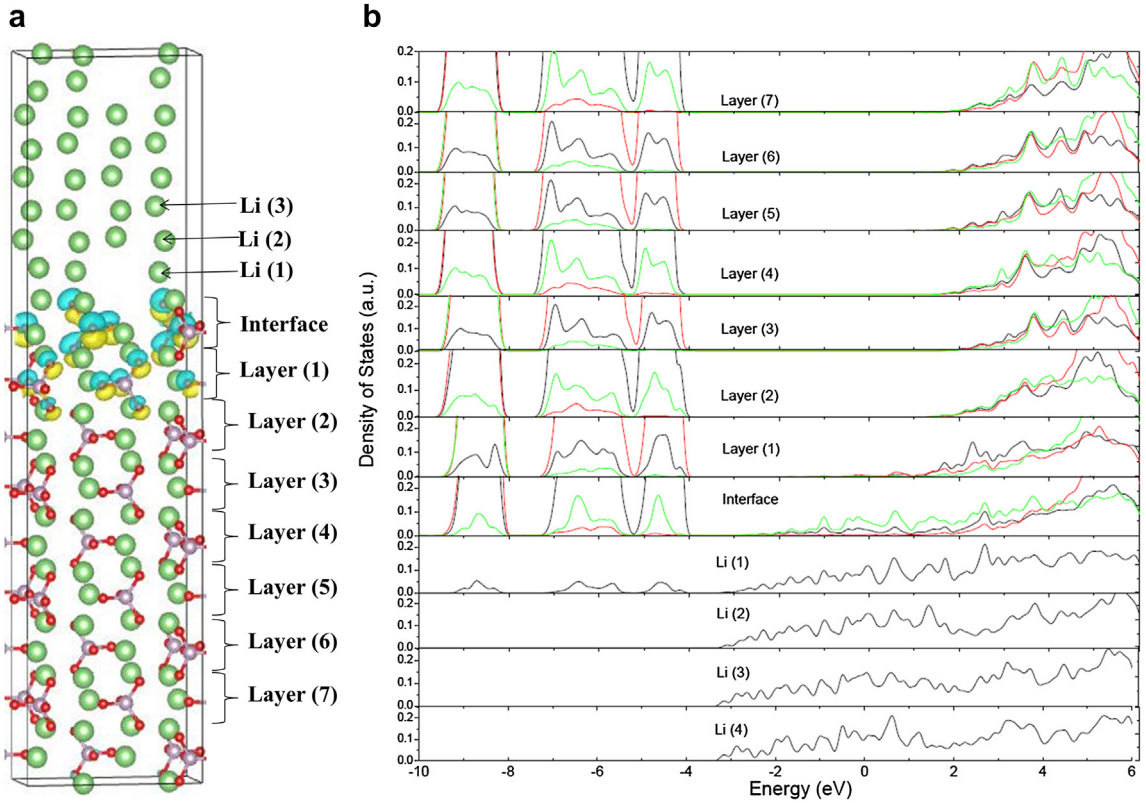

Fig. 5. (a) 3D plot of the charge difference. Li, P and O atoms are indicated by green, pink, and red spheres, respectively. Yellow (positive) and sky blue (negative) colors indicate the partial charge distribution. The isosurface charge value used in the figure is 3×10^{-2} e Å^{-3}. (b) Local density of states (DOS) projected at various atoms and at different layers away from the interface. The Fermi level is located at zero energy and Li, P, and O DOS are represented by black, green and red curves, respectively (For interpretation of the references to color in this figure legend, the reader is referred to the web version of this article.).

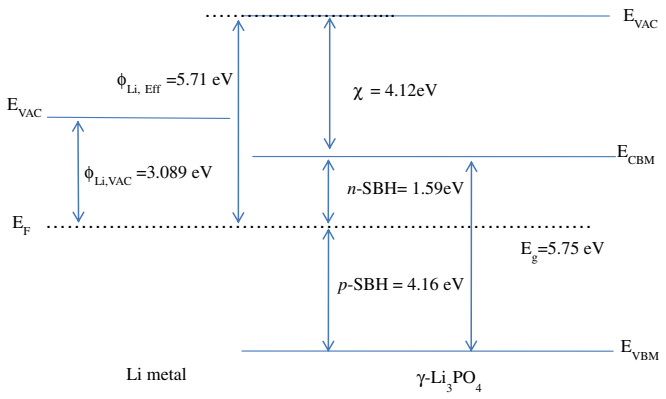

Fig. 6. Schematic energy diagram of the Li/Li_3PO_4 interface. $\phi_{Li,VAC}$, $\phi_{Li,Eff}$ are vacuum work function and effective work function of Li, χ is electron affinity, E_F is the Fermi level, E_{CBM}, E_{VBM}, are conduction band minimum and valance band maximum energies, p-SBH and n-SBH are the Schottky p-type and n-type barrier heights, and E_{VAC} is the vacuum level.

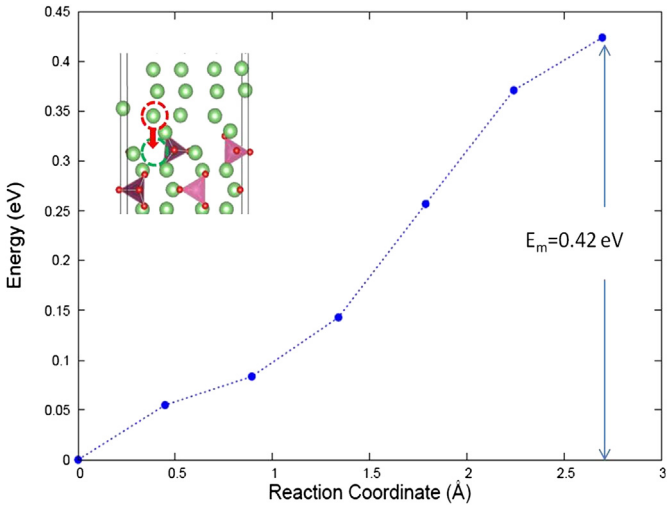

Fig. 7. Migration energy profile of the Li diffusion. E_m is the Li migration barrier between initial and final configuration. The Li diffusion pathway is shown in the inset.

nanometers and in the presence of an external electric field [59]. Thus, space-charge limited electronic conduction shorts anode and cathode electrodes directly through the electrolyte. Hence, there is a need of additional research to understand the downscaling phenomena for the future design of three dimensional lithium ion batteries.

Fig. 6 shows the schematic energy diagram of the Li/Li_3PO_4 interface, as calculated in this work. The electron injection in an electric field from metal to the conduction band of the electrolyte is controlled by the offset between the Fermi level and Schottky barrier height (SBH) for electrons. Comparing the valance band maximum (VBM) and conduction band minimum (CBM) in the diagram with respect to the Fermi level, we can estimate the band offsets of the metal–electrolyte interface. Our results show that the SBH of p-type is ~4 eV and that of n-type is ~2 eV. Therefore, electrons experience a huge barrier to migrate toward the electrolyte through the interface. The calculated work function of Li metal is ~3 eV which is consistent with the experimental value [60], while that of the interface, called effective work function ($\phi_{Li,Eff} = \chi + E_g -$ VBO or {p-SBH}) at the interface between Li and Li_3PO_4 is 5.7 eV. The calculated electron affinity (χ) of the Li_3PO_4 electrolyte is 4.12 eV.

Within this interface model, the Li atom from the metal electrode releases an electron at the interface and the Li^+ will migrate through the electrolyte. The electron needs to flow toward the load through the external circuit from the anode whereas the Li^+ migrates toward the cathode during the discharge cycle. During the charge cycle, Li^+ reverses its direction from the cathode material through the electrolyte to the anode. Li^+ at the interface meets with the electron, is neutralized and penetrates inside the Li anode. To the best of our knowledge, our work is the first detailed study at the atomic level on the electronic structure and mechanisms of ion transport at the electrode/solid electrolyte interface of Li-ion batteries.

3.3. Li migration energy

We have also investigated the migration energy barrier between a Li coming from the electrode (Fig. 7, red circle) to an interstitial site (Fig. 7, green circle) inside the electrolyte. The initial Li migration energy for Li ions between Li anode side (red circle of Fig. 2(b)) to the closest Li interstitial site at the electrolyte (labeled (1) in Fig. 2(b)) is 0.42 eV. The Li migration energy for the Li anode side (red circle) to an interstitial site inside the electrolyte (as, *e.g.*, the one labeled (3) in Fig. 2(b)) is 0.51 eV. Thus, the Li migration from Li anode side to the interstitial side deep inside the electrolyte is at least 0.51 eV. We have computed the Li migration barrier (≈0.3 eV) from an interstitial site to its neighboring site inside the electrolyte which is consistent with previously reported value for the bulk Li_3PO_4 [15]. The activation energies ($E_A = 1/2E^f + E_m$) for the site (1), site (2) and site (3) are 0.20, 0.91 eV and 1.50 eV, respectively taking into account the calculated formation energy of the vacancy–interstitial pair defects corresponding to various Li interstitial sites in the electrolyte and for a Li vacancy in the metal anode side (see Table 1). It indicates that the higher activation energy for Li in the Li metal/Li_3PO_4 interface is due to the high Li defect formation energy of the electrolyte. Our calculations are comparable to available activation energies (1.2–1.3 eV) for bulk polycrystalline samples of γ-Li_3PO_4 [11,61] (For interpretation of the references to color in this paragraph, the reader is referred to the web version of this article.).

We have considered an abrupt and an ideal interface between Li and Li_3PO_4 for the present study. However, including a SEI layer between electrode and electrolyte surfaces and studying its influence on Li ion migration mechanisms would be also interesting. Recent work on Li diffusion in solid electrolyte interphase (SEI) layer Li_2CO_3 indicates that diffusion via a knockoff mechanism to maintain higher O-coordination is more likely to happen, instead of direct hopping from one interstitial site to another interstitial site in Li_2CO_3 [62]. Thus, it may influence the Li ion migration mechanisms in our interface model. Thus, a more comprehensive research on the interface phenomena between electrodes and electrolytes is essential for achieving a breakthrough in battery development. Our study of electrode/electrolyte interface modeling provides useful insights into Li/γ-Li_3PO_4 interfacial phenomena, which will be useful for all-solid-state Li-ion batteries.

4. Summary

In conclusion, we have performed first-principles calculations of defects and interfacial properties in electrode/electrolyte interface (Li/γ-Li_3PO_4). The Li vacancy–interstitial pair defect formation energy in our interface model ranges from 0.82 to 1.93 eV. The low ionic conductivity of the interface arises from the high defect formation energy in the electrolyte, which can be reduced by tuning the metal chemical potential by Li alloying and/or electrolyte doping with suitable elements. Although, further studies are required to elucidate the possible techniques to overcome the high

Li migration barrier and defect formation energies across the interface between electrodes and electrolytes, our study of the Li metal/electrolyte interface provides an important insight into Li-ion migration mechanisms across the interface and shows a research direction to improve its ionic conductivity for future battery applications.

Acknowledgment

Calculations were done in the Texas Advanced Computer Center (TACC) facility. K.C. was supported by the NRF of Korea through WCU program (Grant No. R-31-2009-000-10083-0).

References

[1] M. Armand, J.M. Tarascon, Nature 451 (2008) 652.
[2] A. Patil, V. Patil, D.W. Shin, J.W. Choi, D.S. Paik, S.J. Yoon, Mater. Res. Bull. 43 (2008) 1913–1942.
[3] P. Knauth, Solid State Ionics 180 (2009) 911–916.
[4] M. Armand, Solid State Ionics 69 (1994) 309–319.
[5] T. Minami, A. Hayashi, M. Tatsumisago, Solid State Ionics 177 (2006) 2715–2720.
[6] T. Takahashi, Mater. Sci. Eng., B 13 (1992) 199–202.
[7] J.B. Bates, N.J. Dudney, G.R. Gruzalski, R.A. Zuhr, A. Choudhury, D.F. Luck, J.D. Robertson, Solid State Ionics 647 (1992) 53–56.
[8] J.B. Bates, N.J. Dudney, G.R. Gruzalski, R.A. Zuhr, A. Choudhury, D.F. Luck, J.D. Robertson, J. Power Sources 103 (1993) 43–44.
[9] Y.A. Du, N.A.W. Holzwarth, Phys. Rev. B 81 (2010) 184106.
[10] X. Yu, J.B. Bates, J.G.E. Jellison, F.X. Hart, J. Electrochem. Soc. 144 (1997) 524.
[11] B. Wang, B.C. Chakoumakos, B.C. Sales, B.S. Kwak, J.B. Bates, J. Solid State Chem. 115 (1995) 313.
[12] N. Kamaya, K. Homma, Y. Yamakawa, M. Hirayama, R. Kanno, M. Yonemura, T. Kamiyama, Y. Kato, S. Hama, K. Kawamoto, A. Mitsui, Nat. Mater. 10 (2011).
[13] S. Skaarup, K. West, B. Zachau-Christiansen, Solid State Ionics 28–30 (1988) 975–978.
[14] Y.A. Du, N.A.W. Holzwarth, J. Electrochem. Soc. 154 (11) (2007) A999–A1004.
[15] Y.A. Du, N.A.W. Holzwarth, Phys. Rev. B 76 (2007) 174302.
[16] H.C. Liu, S.K. Yen, J. Power Sources 159 (2006) 245.
[17] L. Popović, B. Manoun, D. de Wall, M.K. Nieuwoudt, J.D. Comins, J. Raman Spectrosc. 34 (2003) 77.
[18] C. Ibarra-Ramírez, M.E. Villafuerte-Castrejón, A.R. West, J. Mater. Sci. 20 (1985) 812.
[19] Y.N. Xu, W.Y. Ching, Y.M. Chiang, J. Appl. Phys. 95 (2004) 6583.
[20] N.D. Lepley, N.A.W. Holzwarth, ECS Trans. 35 (14) (2011).
[21] M. Dollé, L. Sannier, B. Beaudoin, M. Trentin, J.M. Tarascon, Electrochem. Solid-State Lett. 5 (2002) A286.
[22] G. Adachi, N. Imanaka, H. Aono, Adv. Mater. 8 (1996) 127.
[23] A.D. Robertson, A.R. West, A.G. Ritchie, Solid State Ionics 104 (1) (1997).
[24] T. Brousse, P. Fragnaud, R. Marchand, D.M. Schleich, O. Bohnke, K. West, J. Power Sources 68 (1997) 412.
[25] S. Stramare, V. Thangadurai, W. Weppner, Chem. Mater. 15 (2003) 3974.
[26] F. Mizuno, A. Hayashi, K. Tadanaga, M. Tatsumisago, Adv. Mater. 17 (2005) 918.
[27] Y.H. Rho, K. Kanamura, J. Power Sources 158 (2006) 1436.
[28] N.A.W. Holzwarth, et al., J. Power Sources 196 (2011).
[29] A.K. Ivanov-Shitz, V.V. Kireev, O.K. Mel'nikov, L.N. Demainets, Crystallogr. Rep. 46 (5) (2001) 864–867.
[30] Y.-W. Hu, I.D. Raistrick, R.A. Huggins, J. Electrochem. Soc. 124 (1977) 1240.
[31] M. Kotobuki, Y. Suzuki, H. Munakata, K. Kanamura, Y. Sato, K. Yamamoto, T. Yoshida, Electrochim. Acta 56 (2011) 1023–1029.
[32] K. Kishida, J. Mater. Res. 25 (2010).
[33] E. Kobayashi, L.S. Plashnitsa, T. Doi, S. Okada, J. Yamaki, Electrochem. Commun. 12 (2010) 894–896.
[34] N. Kuwata, N. Iwagami, Y. Tanji, Y. Matsuda, J. Kawamura, J. Electrochem. Soc. 157 4 (2010) A521–A527.
[35] M. Park, X. Zhang, M. Chung, G.B. Less, A.M. Sastry, J. Power Sources 195 (2010) 7904–7929.
[36] G. Kresse, J. Furthmuller, J. Comput. Mater. Sci. 6 (1) (1996) 15–50.
[37] R.G. Parr, W. Yang, Density-Functional Theory of Atoms and Molecules, Oxford University Press, New York, 1989.
[38] P. Hohenberg, W. Kohn, Phys. Rev. 136 (1964) B864.
[39] W. Kohn, L.J. Sham, Phys. Rev. 140 (1965) A1133.
[40] S. Lebe`gue, B. Arnaud, M. Alouani, P.E. Bloechl, Phys. Rev. B 67 (15) (2003) 155208.
[41] M. Shishkin, G. Kresse, Phys. Rev. B 74 (3) (2006) 035101.
[42] M. Shishkin, G. Kresse, Phys. Rev. B 75 (2007) 235102.
[43] J.P. Perdew, K. Burke, M. Ernzerhof, Phys. Rev. Lett. 77 (1996) 3865.
[44] J.P. Perdew, K. Burke, M. Ernzerhof, Phys. Rev. Lett. 78 (1997) 1396.
[45] J.P. Perdew, J.A. Chevary, S.H. Vosko, et al., Phys. Rev. B 42 (1992) 6671.
[46] H. Jonsson, G. Mills, K.W. Jacobsen, Classical and Quantum Dynamics in Condensed Phase Simulations, World Scientific, Singapore, 1998.
[47] M. Leslie, M.J. Gillan, J. Phys. C Solid State Phys. 18 (1985) 973.
[48] C.G. Van de Walle, A. Janotti, Phys. Status Solid B (2010) 1–9.
[49] C.G. Van de Walle, J. Neugebauer, J. Appl. Phys. 95 8 (2004) 15.
[50] W. Li, G. Wu, C.M. Araujo, R.H. Scheicher, A. Blomqvist, R. Ahuja, Z. Xiong, Y. Feng, P. Chen, Energy Environ. Sci. 3 (2010) 10.
[51] M. Wachtler, J.O. Besenhard, M. Winter, J. Power Sources 94 (2001) 189.
[52] Y. Kwon, H. Kim, S.-G. Doo, J. Cho, Chem. Mater. 19 (2007) 982–986.
[53] W.B. Xing, A.M. Wilson, K. Eguchi, G. Zank, J.R. Dahn, J. Electrochem. Soc. 144 (1997) 2410.
[54] M. Winter, J.O. Besenhard, Electrochim. Acta 45 (1999) 31.
[55] Y. Liu, et al., J. Power Sources 146 (2005) 376–379.
[56] W. Tang, E. Sanville, G. Henkelman, J. Phys.: Condens. Matter 21 (2009) 084204.
[57] E. Sanville, S.D. Kenny, R. Smith, G. Henkelman, J. Comput. Chem. 28 (2007) 899–908.
[58] G. Henkelman, A. Arnaldsson, H. Jónsson, Comput. Mater. Sci. 36 (2006) 254–360.
[59] D. Ruzmetov, et al., Nano Lett. 12 (2012) 505–511.
[60] D.R. Lide (Ed.), CRC Handbook of Chemistry and Physics, 88th ed., CRC Press, Boca Raton, FL, 2008.
[61] R.A. Huggins, Electrochim. Acta 22 (1977) 773.
[62] S. Shi, P. Lu, Z. Liu, Y. Qi, L.G. Hector Jr., H. Li, S.J. Harris, J. Am. Chem. Soc. 134 (2012) 15476–15487.